THE JOURNAL OF PHYSICAL CHEMISTRY C

Article

pubs.acs.org/JPCC

Enhanced Stability of Rubrene against Oxidation by Partial and Complete Fluorination

F. Anger,[†] T. Breuer,[‡] A. Ruff,[§,⊥] M. Klues,[‡] A. Gerlach,[†] R. Scholz,[∥] S. Ludwigs,[§] G. Witte,[‡] and F. Schreiber*[,†]

[†]Institut für Angewandte Physik, Universität Tübingen, Auf der Morgenstelle 10, 72076 Tübingen, Germany

[‡]Fachbereich Physik, Universität Marburg, Renthof 7, 35032 Marburg, Germany

[§]Institut für Polymerchemie (IPOC), Universität Stuttgart, Pfaffenwaldring 55, 70569 Stuttgart, Germany

[∥]Institut für Angewandte Photophysik, TU Dresden, George-Bähr-Straße 1, 01069 Dresden, Germany

Supporting Information

ABSTRACT: We report on the oxidation potential of partially fluorinated ($C_{42}F_{14}H_{14}$, F_{14}-RUB) and perfluorinated rubrene ($C_{42}F_{28}$, PF-RUB) studied by cyclic voltammetry (CV) in solution as well as by spectroscopic ellipsometry and near edge X-ray absorption fine structure (NEXAFS) spectroscopy in thin films in combination with density functional theory computations. Due to their different electronic structure, the fluorinated derivatives have a higher oxidation potential and are more stable than rubrene ($C_{42}H_{28}$, RUB).

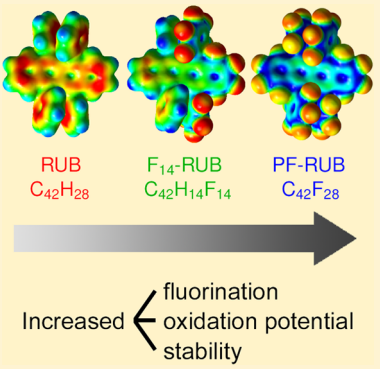

INTRODUCTION

Rubrene (5,6,11,12-tetraphenyltetracene, $C_{42}H_{28}$, RUB) is among the most promising materials for applications based on organic semiconductors,[1] at least due to its high charge carrier mobility.[2−5] One of the challenges in organic and hybrid electronics concerns the stability against exposure to ambient gases, including in particular oxygen.[6,7] This is especially relevant for thin films, which are easier to produce than single crystals and thus more attractive for applications, but can often exhibit a more grainy morphology which allows oxygen to penetrate into the material.[8−11] A possibility to address this issue is to modify the rubrene molecule by substitution with different elements or side groups in order to reduce its susceptibility to oxidation.[12−16] Partial or complete fluorination is a typical strategy in this context, since the large electronegativity of fluorine is expected to hinder oxidation very effectively.[17,18] Furthermore, fluorination will also change the electronic and optical properties of a material,[19,20] which also is of relevance for the interface between organic compounds in applications.[21−23]

In this study, we examine to which extent rubrene can be stabilized by (per)fluorination and how this chemical modification affects the desirable optical as well as electronic spectra. For this purpose, the newly synthesized perfluoro-5,6,11,12-tetraphenyltetracene ($C_{42}F_{28}$, PF-RUB) and 1,2,3,4-tetrafluoro-5,12-bis(2,3,4,5,6-pentafluorophenyl)-6,11-diphenyltetracene ($C_{42}F_{14}H_{14}$, F_{14}-RUB) shown in Figure 1, both excellent candidates for a systematic investigation, are studied using cyclic voltammetry (CV), spectroscopic ellipsometry, and near edge X-ray absorption fine structure (NEXAFS). Together with density functional theory (DFT), we evaluate the experimental results of the fluorinated compounds in solution and thin films with unsubstituted rubrene itself. A comparison of the experimental and DFT results obtained for the fluorinated compounds in solution and thin films provides a consistent picture of the stabilization mechanism.

EXPERIMENTAL SECTION

Pristine RUB was purchased from Acros, while the fluorinated rubrenes were synthesized by Sakamoto and Suzuki.[25] All materials were purified by temperature gradient sublimation.

Cyclic voltammograms were recorded with a PGSTAT101 potentiostat from Metrohm (Filderstadt, Germany) under argon atmosphere in a gastight three electrode cell. The working electrode consisted of a Pt disk (nominal diameter d = 1 mm) sealed in glass. A Pt wire was used as the counter electrode. An Ag wire coated with an AgCl-layer which was directly immersed into the electrolyte solution served as (pseudo)reference electrode. All potentials are given versus the formal potential of the redox couple Fc/Fc^+ (ferrocene/ferrocenium).[26] Fc was used as internal standard (added after substrate measurements). Voltammograms were recorded in deaerated (argon bubbling) CH_2Cl_2 containing NBu_4PF_6 acting as the supporting electrolyte

Received: December 15, 2015
Revised: February 2, 2016
Published: March 3, 2016

ACS Publications © 2016 American Chemical Society

DOI: 10.1021/acs.jpcc.5b12293
J. Phys. Chem. C 2016, 120, 5515−5522

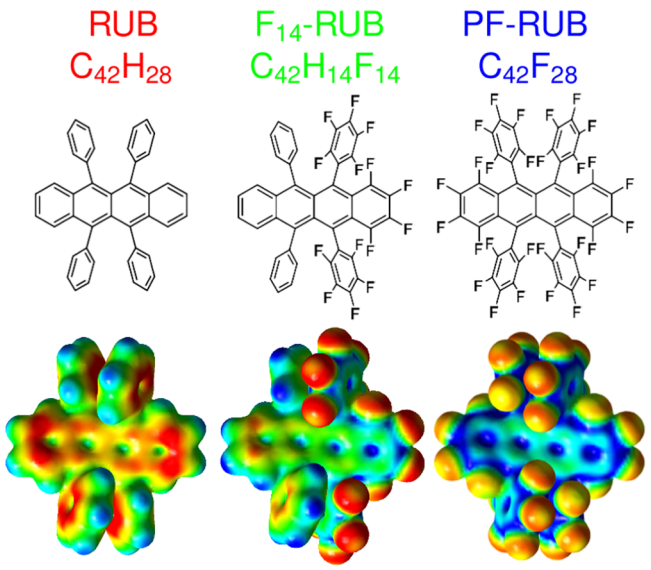

Figure 1. Chemical structure and molecular electrostatic potential (MEP) plot of the compounds investigated (from left to right) rubrene (RUB, $C_{42}H_{28}$), partially fluorinated rubrene (F_{14}-RUB, $C_{42}F_{14}H_{14}$), and perfluorinated rubrene (PF-RUB, $C_{42}F_{28}$).[24]

(0.1 M). CH_2Cl_2 was dried prior to use with activated Al_2O_3 (dried at 80 °C for several days in an oven). Cyclic voltammograms were not background corrected. For the estimation of half wave potentials voltammograms recorded with 100 mV/s were used. Half wave potentials $E_{1/2}$ of the redox couple were calculated from the peak potentials of the oxidation E_p^{ox} and reduction E_p^{red} as $E_{1/2} = (E_p^{ox} + E_p^{ox})/2$. Substrate concentrations were 2.6 mM in the case of RUB and 1.4 mM for F_{14}-RUB and PF-RUB.

The ionization potential (IP) and electron affinity (EA) of the RUB, F_{14}-RUB, and PF-RUB molecules in solution were computed with the B3LYP functional and triple-ζ valence plus polarization (TZVP) basis set using Turbomole 6.4.[27] The values for IP and EA of the RUB and PF-RUB (F_{14}-RUB) molecules in D_2 (C_2) symmetry were estimated from the energies of the ionized species under the consideration of the polarization energy of the solvent (CH_2Cl_2).

Thin films of the three materials were deposited at room temperature under high vacuum conditions on silicon wafers covered by a native oxide layer. By keeping the molecular flux at a constant rate of 1.1 Å/min monitored by a quartz crystal microbalance (QCM), films with thicknesses of 20 nm were prepared. Under these conditions RUB, F_{14}-RUB, and PF-RUB are known to form amorphous thin films.[24] About 90 min after thin film deposition, air was leaked into the UHV chamber up to a pressure of 50 mbar. Real-time data of the oxidation process were obtained using spectroscopic ellipsometry with a broad band Xe lamp (75 W, 250−1000 nm), while the samples were exposed to air.[28] The ellipsometer (Wollam M-2000 SE) was equipped with a rotating compensator for accurate measurement of the polarization and a CCD camera enabling simultaneous detection of all wavelengths, which allows minimization of the acquisition time (t = 1 min). In order to measure the samples in situ, the ellipsometer was mounted on the vacuum system with strain free quartz windows resulting in a fixed angle of incidence of ~61°. Data acquisition started directly with the partial venting process of the vacuum system until after 4−10 min a pressure of 50 mbar was reached, which then was kept constant.

Near edge X-ray absorption fine structure (NEXAFS) spectra were obtained from thin films of F_{14}-RUB and PF-RUB that were deposited in ultrahigh vacuum with similar growth parameters as above. Prior to the measurements, the thin films had been exposed to air for several days as the low amount of available material did not allow for the in situ preparation of an additional batch of samples. The measurements were performed at the HE-SGM dipole beamline of the synchrotron BESSY II in Berlin (Germany) providing linearly polarized light (polarization factor = 0.91) and an energy resolution at the carbon K-edge of about 300 meV. All NEXAFS spectra were recorded in partial electron-yield mode using a channel-plate detector with a retarding field of −150 V. For the calibration of the absolute energy scale, the photocurrent from a carbon-coated gold grid in the incident beam (absorption maximum = 284.9 eV) was recorded simultaneously. In order to determine the average molecular orientation relative to the sample surface, NEXAFS spectra were recorded at different angles of incidence (θ = 30°, 55°, 70°, and 90°). The observed dichroism was analyzed after flux normalization and considering the transmission of the monochromator.

Computations of C 1s NEXAFS spectra were performed on the Slater transition state level by optimizing the molecular geometry using the gradient-corrected revised Perdew−Burke−Ernzerhof (RPBE) functional and all-electron TZVP basis sets. Subsequently, the excited states for each nonsymmetry equivalent excitation center, i.e., carbon atom, were calculated separately. In this step, the excitation center is modeled using an IGLO-III basis set which allows the description of inner shell relaxation effects, while the other carbon centers are described by effective core potentials (ECPs). Further details on the computations can be found in previous work.[29,30]

RESULTS

Electrochemical Properties in Solution. Electrochemical methods such as CV allow for the investigation of the general electrochemical properties of a redox-active compound. Both, oxidation and reduction processes at the electrode interface can be examined by means of the same method, including the determination of redox potentials.[31] Moreover, from the potential values of the corresponding oxidative or reductive processes, values for the energy levels of the highest occupied molecular orbital (HOMO) and the lowest unoccupied molecular orbital (LUMO) can be estimated.[32]

The redox behavior, including the determination of the redox potentials, of RUB, F_{14}-RUB, and PF-RUB in solution and the absence of oxygen was studied by means of CV in 0.1 M NBu_4PF_6/CH_2Cl_2 at a Pt disk electrode under planar diffusion conditions. Cyclic voltammograms of RUB (Figure 2a) show a first chemically reversible oxidation (solid line, cation formation) and a chemically reversible reduction (dashed line, anion formation) with peak potentials for the oxidation (E_p^{ox}) and the reduction (E_p^{red}) of +0.39 and −2.16 V, respectively. The half wave potentials of the anodic and cathodic redox couple are found at +0.33 ($E_{1/2}^{ox}$, oxidation) and −2.09 V ($E_{1/2}^{red}$, reduction). Both values are in good agreement with previously reported data.[12,16,17,33] At higher potentials, a second chemically irreversible oxidation (formation of the dication) wave located at around +1.0 V[16] is observed (see the Supporting Information).

The anodic and cathodic I−E curves of the partially fluorinated F_{14}-RUB (Figure 2b) show a chemically reversible oxidation (solid line, cation formation) and a chemically reversible reduction (dashed line, anion formation) with half wave potentials of $E_{1/2}^{ox}$ = +0.91 V and $E_{1/2}^{red}$ = −1.55 V. At lower

DOI: 10.1021/acs.jpcc.5b12293
J. Phys. Chem. C 2016, 120, 5515−5522

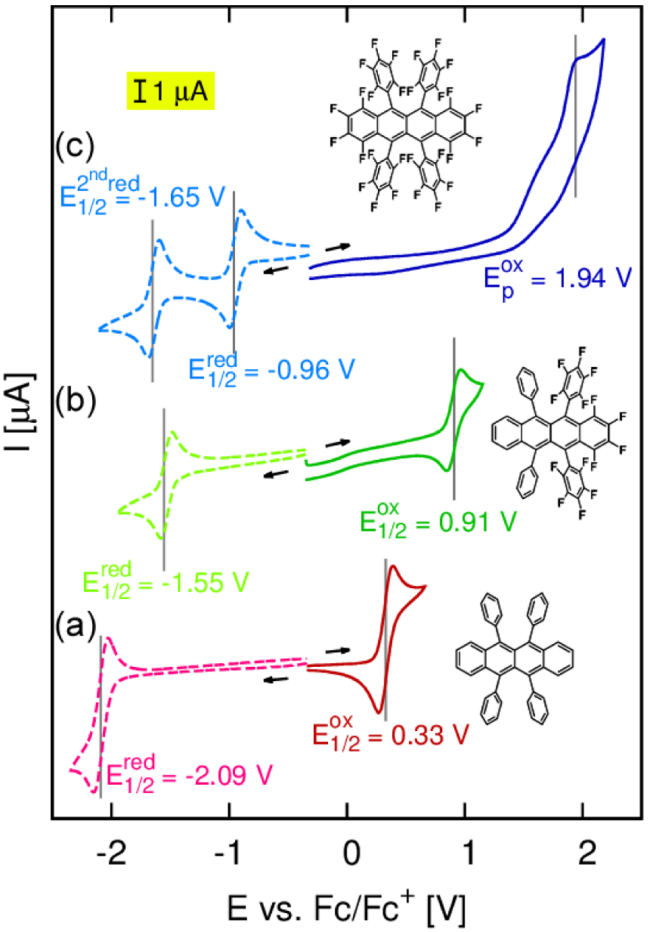

Figure 2. Anodic (solid lines) and cathodic (dashed lines) cyclic voltammograms of RUB (a), c = 2.3 mM, F_{14}-RUB (b), c = 1.4 mM, and PF-RUB (c), c = 1.4 mM, in 0.1 M NBu_4PF_6/CH_2Cl_2 at Pt recorded with a scan rate of ν = 100 mV s^{-1}. Arrows indicate scan direction, anodic and cathodic I–E curves were recorded separately, voltammograms were not background corrected. The shoulder in (c) located at around +1.6 V is attributed to impurities in the electrolyte (revealed by measuring the background current in the absence of substrate).

potentials a chemically irreversible redox wave at around −2.15 V is visible, which becomes chemically reversible for fast scan rates. This process relies on a decomposition within the time scale of the experiment (see the Supporting Information).

Cyclic voltammograms of PF-RUB (Figure 2c) show two chemically reversible reduction processes with half wave potentials of −0.96 V and −1.65 V. We attribute the two redox processes to the stepwise formation of the dianion via an anionic species. In contrast to F_{14}-RUB, the dianionic species formed during the second reduction of PF-RUB (−1.65 V) seems to be more stable within the time scale of the voltammetric experiment. The second electron transfer process is chemically reversible even at slow scan rates ($\nu \leq$ 200 mV s^{-1}). A chemically irreversible oxidation wave at considerably high potentials (close to the limit of the potential window of the electrolyte, Figure 2c, solid line) is revealed by the anodic potential cycle of PF-RUB. The peak potential of the oxidation is +1.94 V (ν = 100 mV s^{-1}).

An increase in the degree of fluorination leads to an increase of the oxidation potentials of +1.6 V when going from RUB (+0.33 V) via F_{14}-RUB (+0.91 V) to PF-RUB (+1.94 V), because of the electron withdrawing effect of the fluorine atoms that are attached to the RUB core. Simultaneously, the reduction potential increases by about +1.1 V from −2.09 V (RUB) to −0.96 V (PF-RUB) for the same reason. The systematic tuning of the molecular energy levels by different degrees of fluorination has also been shown for other small molecule organic semiconductors, such as phtalocyanines.[34] Indeed, the perfluorinated compound PF-RUB is thermodynamically more stable against oxidation (high oxidation potential, low HOMO level) than F_{14}-RUB and much more stable than RUB, but is readily reduced (high reduction potential, low LUMO level).

Under the assumption that the redox couple Fc/Fc^+ (redox potential standard[26]) is located at −5.1 eV in the Fermi energy scale,[32] the HOMO (E^{exp}_{HOMO}) and LUMO (E^{exp}_{LUMO}) energy values of RUB, F_{14}-RUB and PF-RUB can be estimated from the half wave potentials of the oxidation and the first reduction according to

$$E^{exp}_{HOMO} = -(E^{ox}_{1/2} + 5.1)[eV] \quad (1)$$

$$E^{exp}_{LUMO} = -(E^{red}_{1/2} + 5.1)[eV] \quad (2)$$

As follows from the redox potentials, PF-RUB has the lowest HOMO (−7.0 eV) and lowest LUMO (−4.1 eV) level whereas RUB exhibits the highest HOMO (−5.4 eV) and highest LUMO (−3.0 eV) level. Note that the HOMO of PF-RUB may be slightly overestimated since the peak potential was used instead of the half wave potential. The energy level of the partially fluorinated compound F_{14}-RUB is located between the values for the other two compounds, at E^{exp}_{HOMO} = −6.0 eV and E^{exp}_{LUMO} = −3.6 eV, which is in good agreement with recent observations obtained with photoelectron spectroscopy in the solid state.[35] Hence, we find for both fluorinated compounds, F_{14}-RUB and PF-RUB, that the oxidation potentials lie above the ionization potentials (IPs) of most other RUB derivatives studied so far.[12,14−16]

Optical Absorption of Thin Films. Figure 3 shows real-time absorption spectra (ε_2) that were obtained during exposure to air using spectroscopic ellipsometry from thin films of RUB, F_{14}-RUB, and PF-RUB with a thickness of 20 nm, each. The ellipsometric raw data consisting of the parameters Ψ and Δ was converted into the dielectric function $\varepsilon_1 + i\varepsilon_2$ using a commercial software package (WVASE32). The data was modeled with an isotropic layer accounting for the organic thin film deposited on the native silicon wafer, which in each case is represented by a silicon and a dioxide layer, respectively. The spectra shown in Figure 3a−c were acquired in intervals of 100 min beginning with the exposure to air at a pressure of 50 mbar into the vacuum chamber. The time resolution of the experiment was determined by their integration time of 1 min.

At t = 0 min (still under vacuum conditions) we observe the HOMO−LUMO transition of the unoxidized RUB, F_{14}-RUB, and PF-RUB thin films at 2.34, 2.30, and 2.33 eV, respectively, which is in good agreement with previously reported values for the optical gap.[35] All compounds show a pronounced vibronic progression of the HOMO−LUMO transition that can be well fitted with a spacing of ∼0.16 eV.[24] For RUB, we find an additional peak at 4.03 eV[28] that essentially relies on the HOMO-(LUMO+1) transition. For the fluorinated materials F_{14}-RUB and PF-RUB, we find analogous transitions at 3.95 and 4.03 eV, respectively.

These observations clearly show that the relative energy alignment of the three materials is remarkably similar, merely the optical transitions of F_{14}-RUB are slightly red-shifted by 0.05 eV compared to PF-RUB and RUB.[24] This evidences that the optical properties of the compounds do not change fundamentally with

DOI: 10.1021/acs.jpcc.5b12293
J. Phys. Chem. C 2016, 120, 5515−5522

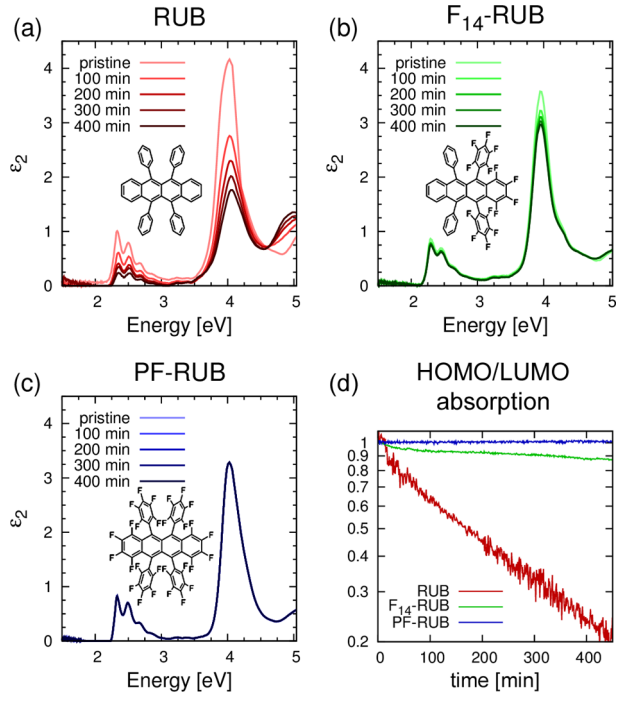

Figure 3. Real-time observation of the optical properties (ε_2) of (a) RUB, (b) F_{14}-RUB, and (c) PF-RUB thin films using spectroscopic ellipsometry. 90 min after deposition (20 nm), the thin films were exposed to air (50 mbar). (d) Time dependent intensity of the HOMO-LUMO transition of the thin films shown in (a–c). The respective intensities are normalized to the value before exposure to oxygen at $t = 0$ min. While the intensity of RUB decreases exponentially to almost 20% after 400 min[13,28] (strong oxidation effects resulting in bleaching), there is almost 90% of the initial intensity observed for F_{14}-RUB. For PF-RUB no change can be measured within the time scale of the experiment.

the degree of fluorination, which is in contrast to perfluorinated acenes like pentacene or tetracene, where fluorination results in a notable redshift of the respective HOMO–LUMO transition.[19,36] However, the ionization potential of thin films of the fluorinated rubrenes was shown to differ by ~0.9 eV and ~1.7 eV from RUB to F_{14}-RUB and PF-RUB, respectively.[35]

It is well-known that RUB becomes transparent in the visible spectral region upon exposure to light and oxygen since photooxidation leads to the formation of transparent rubrene-endoxide or -peroxide.[7,13,28,37] In good agreement with this expectation, we observe an exponential distinct decrease in intensity of the HOMO–LUMO transition of RUB when permitting air to enter the vacuum system (Figure 3d). Simultaneously, the transition at ~4 eV is getting weaker, and a new transition at ~5 eV related to photooxidized RUB exhibits increased intensity.[28]

For F_{14}-RUB, the observed change in the absorption spectra is qualitatively similar to that observed for RUB; however, it is considerably less pronounced. The intensity decrease of the HOMO–LUMO transition and also of the transition at ~4.03 eV is clearly less pronounced than for RUB. As a result, the residual absorption signal after 400 min is still stronger than that which is found only after 100 min for RUB with respect to the initial signals, indicating a reduced susceptibility to oxygen. In contrast to these two cases, we do not observe any changes in the optical spectra of PF-RUB upon exposure to air within the duration of the experiment.

Similarly to RUB, thin films of fluorinated rubrene have been shown to grow disordered on silicon,[24,38] which allows oxygen to penetrate all films. Thus, a stabilizing mechanism due to molecular ordering as it occurs particularly in the bulk of RUB single crystals, where it leads to a reduction of the susceptibility to oxidation due to sterical hindrance,[10] can be neglected. Note, however, that thin films of fluorinated rubrene indeed can dewet during storage, but a possible molecular reordering occurs on a time scale that is expected to be significantly longer than the oxidation process. This demonstrates that F_{14}-RUB is considerably and PF-RUB far more stable against oxidation in comparison to RUB.

Computation of Ionized Molecules. For a more quantitative analysis of the ionization energies of the three compounds, we performed density functional theory (DFT) computations (B3LYP/TZVP) with the quantum chemistry program package Turbomole 6.4.[27] Relying on the ionization potential and electron affinity of the free (gas phase) molecules of the three materials with twisted tetracene backbone,[35] the ionization potential (IP_+^{sol}) and electron affinity (EA_-^{sol}) of the ionized species in solution were estimated via[39,40]

$$IP_+^{sol} = IP_+^{gas} - P_+ \quad \text{and} \quad EA_-^{sol} = EA_-^{gas} + P_- \tag{3}$$

P_+ and P_- designate the polarization energies arising from the embedding into a medium with dielectric constant differing from one. The polarization energies in dichloromethane with dielectric constant $\varepsilon_{Solvent} = 9.08$ is calculated by[41]

$$P_+ = \frac{e^2}{4\pi\varepsilon_0}\frac{1}{2r_{Ion}}\left(1 - \frac{1}{\varepsilon_{Solvent}}\right) \tag{4}$$

where r_{Ion} is the radius of the ionized molecules. For an effective ion radius $r_{Ion} = r_+ = r_- = 7.0$ Å[33] for both cation and anion of all three compounds, eq 4 yields a polarization energy of $P_+ = P_- = 0.92$ eV for the simply ionized molecules. Table 1 summarizes the characteristic potential values and orbital energies of RUB, F_{14}-RUB and PF-RUB derived from cyclic voltammetric experiments and DFT computations. From the experimental E_{HOMO}^{exp} and E_{LUMO}^{exp} values the electrochemical HOMO–LUMO gap was obtained from $E_{gap,CV}^{exp} = E_{LUMO}^{exp} - E_{HOMO}^{exp}$. The comparison of the values for computed potentials with the experimental electrochemical gaps reveals particularly for PF-RUB a very good agreement. For RUB and F_{14}-RUB, the computed gap $E_{gap,CV}^{DFT}$ overestimates $E_{gap,CV}^{exp}$ slightly, which suggests a smaller radius r_{Ion} of the ionized molecules (and hence larger polarization energies) for these two materials compared to PF-RUB. The electrochemical gap $E_{gap,CV}^{exp}$ increases when going from RUB (2.4 eV) to PF-RUB (2.9 eV), which lies slightly above the optical gap $E_{gap,opt}^{exp}$.[24] The high value of PF-RUB is a result of the nonlinear increase of the redox potentials with increasing F-content within the RUB core.

NEXAFS of Thin Films. In order to investigate the electronic structure of the fluorinated rubrenes with respect to their unoccupied states in the processed thin films, X-ray absorption spectroscopy at the carbon K-edge (C 1s-NEXAFS) was applied. Comparing the X-ray absorption spectra detected in partial electron yield (PEY) at different sample orientation (dichroism) also allows us to determine the effective molecular orientation with respect to the surface normal.[44] Figure 4 shows NEXAFS spectra of PF-RUB and F_{14}-RUB that were acquired at different angles of incidence. The observed equal absorption signals at all angles for the F_{14}-RUB and PF-RUB films indicate that the molecules do not exhibit a distinct orientation but are disordered

DOI: 10.1021/acs.jpcc.5b12293
J. Phys. Chem. C 2016, 120, 5515–5522

Table 1. Comparison of Experimental and Computed Orbital and Gap Energies[a]

	RUB	F_{14}-RUB	PF-RUB	
Cyclic voltammetry				
$E_{1/2}^{\text{2nd red}}$		-2.14 ± 0.01[b]	-1.65 ± 0.01	[V]
$E_{1/2}^{\text{red}}$	-2.09 ± 0.01	-1.55 ± 0.01	-0.96 ± 0.03	[V]
$E_{1/2}^{\text{ox}}$	$+0.33 \pm 0.01$	$+0.91 \pm 0.01$	$+1.94$[c]	[V]
$E_{1/2}^{\text{2nd ox}}$	$+1.00 \pm 0.01$	$+1.43 \pm 0.01$		[V]
HOMO and LUMO energies (exp.)				
$E_{\text{LUMO}}^{\text{exp}}$	-3.0	-3.6	-4.1	[eV]
$E_{\text{HOMO}}^{\text{exp}}$	-5.4	-6.0	-7.0[c]	[eV]
Electron affinities and ionization potential (DFT)				
EA_{2-}^{sol}		-2.6	-3.5	[eV]
EA_{-}^{sol}	-2.1	-3.1	-3.9	[eV]
IP_{+}^{sol}	-5.1	-6.0	-6.9	[eV]
IP_{2+}^{sol}	-5.7	-6.5		[eV]
Gap energies				
$E_{\text{gap, CV}}^{\text{exp}}$	2.4	2.4	2.9[c]	[eV]
$E_{\text{gap, CV}}^{\text{DFT}}$	3.0	2.9	3.0	[eV]
$E_{\text{gap, opt}}^{\text{exp}}$	2.3	2.3	2.3	[eV]

[a]Half wave potential values $E_{1/2}^{\text{ox}}$ and $E_{1/2}^{\text{red}}$ derived from cyclic voltammetric experiments in 0.1 M NBu_4PF_6/CH_2Cl_2 at a Pt electrode (ν = 100 mV s^{-1}). All $E_{1/2}$ are vs Fc/Fc^+ and are mean values over several cycles. The resulting $E_{\text{HOMO}}^{\text{exp}}$, $E_{\text{LUMO}}^{\text{exp}}$, and the electrochemical HOMO-LUMO gap $E_{\text{gap,CV}}^{\text{exp}}$ (= $E_{\text{LUMO}}^{\text{exp}} - E_{\text{HOMO}}^{\text{exp}}$) for the three compounds are compared with computed DFT (TZVP/B3LYP) values (see text). For the estimation of the computed LUMO−1 level, a polarization energy $P_{2-} = 4P_{-}$ was used. Values for the optical gap ($E_{\text{gap,opt}}^{\text{exp}}$) obtained from molecules diluted in CH_2Cl_2 are taken from ref 24. [b]Estimated from voltammograms recorded with $\nu \geq 500$ mV s^{-1}. [c]Value of E_{p}^{ox} is used, since the oxidation is chemically irreversible.

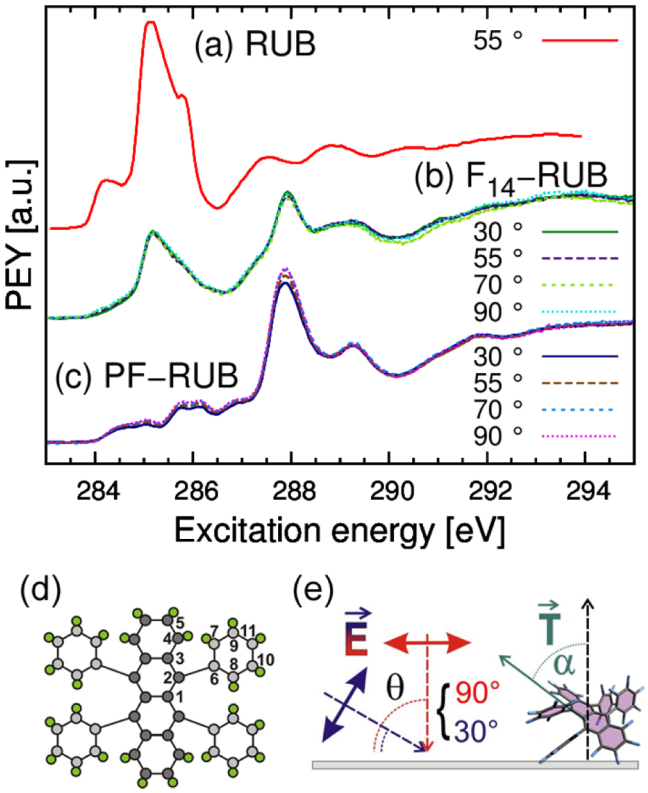

Figure 4. C 1s NEXAFS spectra of (a) RUB, (b) F_{14}-RUB, and (c) PF-RUB taken at different angles of the incident light after several days of exposure to air. The uniformity of the signal intensities at all angles proves the isotropic orientation of the fluorinated molecules in the samples (see text). The data of the unsubstituted RUB was taken from ref 42. (c) Sketch of PF-RUB with indices showing differently coordinated carbon atoms and (d) sketch of experimental setup for the NEXAFS measurements.

or polycrystalline within the film. This is in good agreement with previous results from PF-RUB and F_{14}-RUB thin films.[24,38]

In general, in the absence of a distinct dichroism it cannot directly be discriminated between statistically oriented molecules and molecules with a uniform orientation of 55°,[45] which represents the so-called magic angle where the dichroism disappears.[44] However, since the tetracene backbone and the phenyl side groups exhibit relative twists between each other and both of them yield resonances with different transition dipole moment (TDM) orientation, this allows their individual orientation analysis.[46] Hence, the assumption of a uniform orientation of 55° with respect to the TDM of the tetracene-related excitations would result in a different and distinct dichroism of the phenyl groups. Since, however, constant X-ray absorption is found over the entire energy range, such a situation can safely be ruled out, and the molecules are reliably determined to have no preferential orientation.

In the case of pristine RUB, the NEXAFS spectra were found to be well described by superpositions of the NEXAFS signatures of benzene and tetracene, hence indicating that the electronic system of RUB can be separated into the backbone and side group.[42] Due to the stability of PF-RUB against oxidation, the corresponding spectra can also be analyzed in this form. The NEXAFS resonances at low energies can be correlated to excitations found in pure tetracene, while those at higher energies correspond well to the signature of perfluorobenzene (PF-benzene), cf. Figure 5a.[43] Although the F_{14}-RUB films are only slightly susceptible to oxidation as observed in the optical measurements, a corresponding decomposition of the NEXAFS spectra for F_{14}-RUB is more complicated, since some of the molecules could be significantly modified as it is throughout the case for RUB.[42,47] Indeed, strong modifications of the RUB NEXAFS spectra are observed upon oxidation of corresponding thin films.[48] In particular, the resonances at 284.2 and 285.8 eV (cf. Figure 4a) vanish, leaving behind a major resonance at 285.1 eV.

Upon closer inspection, however, the successful decomposition of PF-RUB into parts resulting from tetracene and perfluorobenzene is surprising. In fact, tetracene is not an ideal choice to be compared to the PF-RUB spectra, since the acene backbone in PF-RUB is significantly altered with respect to pure tetracene. Not only are the carbon atoms at the center position modified in their chemical surrounding due to the attached phenyl side groups (carbon atom 2 and symmetric equivalents in Figure 4), but furthermore is the chemical environment of the carbon atoms 4 and 5 (and the symmetry equivalents) severely changed as a result of the fluorination. The strong electronegativity of the fluorine neighbors leads to an increased ionization potential of the core electrons in these atoms by about 2 eV as it has been found in previous measurements.[35] Following a similar line of argument, also the contributions of the phenyl side groups are expected to differ from pure PF-benzene, which applies particularly to the carbon atoms linked to the tetracene backbone without direct fluorine neighbors. In order to verify these considerations and gain further insights into the actual nature of the signature of the PF-RUB NEXAFS resonances, we performed DFT-computations using the StoBe package,[29] which

DOI: 10.1021/acs.jpcc.5b12293
J. Phys. Chem. C 2016, 120, 5515−5522

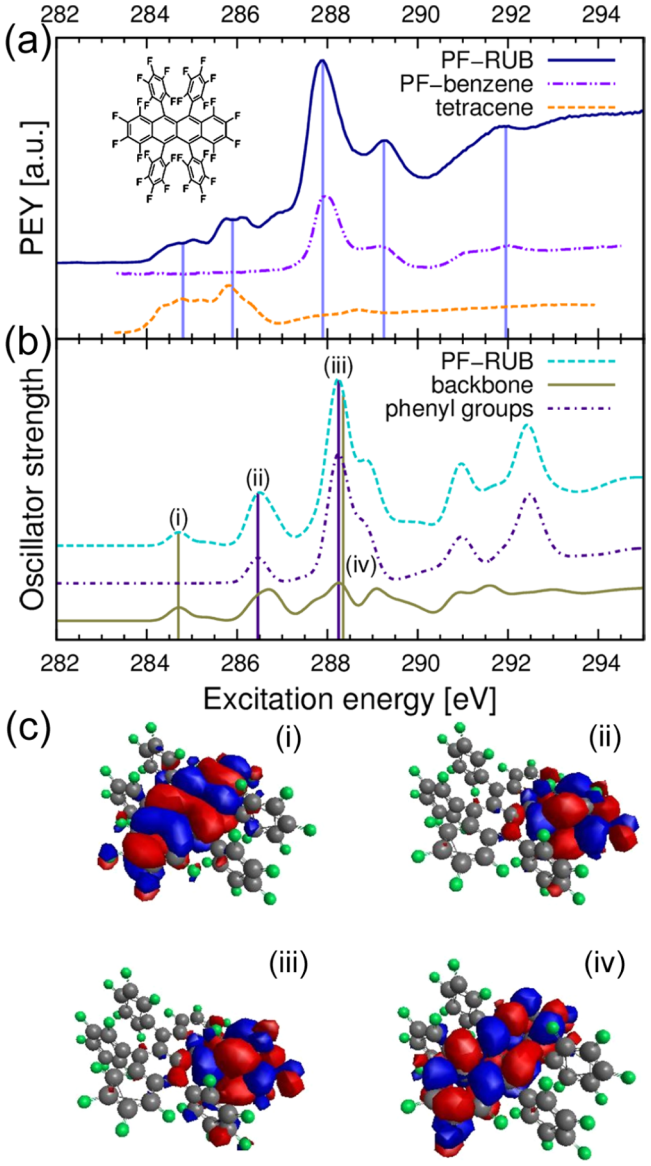

Figure 5. (a) Comparison of the experimental C 1s NEXAFS spectra of PF-RUB, perfluorobenzene (PF-benzene, data taken from ref 43) and tetracene (data taken from ref 42). The spectrum of PF-RUB can be interpreted as a superposition of the latter two. (b) Comparison of the computed spectrum of PF-RUB with separation into the computed contributions from the phenyl groups ((ii) and (iii)) and the tetracene backbone ((i) and (vi)). (c) Visualization of the excited states (i–iv) depicted in (b) showing that the electronic systems of the phenyl groups and the tetracene backbone are strictly separated.

allows the reliable simulation of polycyclic aromatic hydrocarbons and their derivatives.[30] Since in mature PF-RUB thin films molecules with both planar and twisted tetracene backbones may occur,[38] isomers in both D_2 (twisted) and C_{2h} (planar) symmetry[10,42] were considered for the computations. As these results show that the computed spectra of the different species are virtually identical (for details see the Supporting Information), we do not distinguish between the different conformations in the following.

As presented in Figure 5b, the computed spectrum (cyan dashed curve) corresponds nicely to the experiment in Figure 5a. Since oxidation of RUB was shown to significantly modify the NEXAFS signature,[42,48] the remarkably good agreement between experiment and theory supports our finding that the PF-RUB films are stable against oxidation.

Since the computed spectrum represents the sum of all 11 partial NEXAFS spectra for the inequivalent individual excitation centers (i.e., carbon atoms), this data can be easily separated into one spectrum representing the contributions from carbon atoms in the phenyl rings (purple dashed curve) and another one with the peaks corresponding to excitation centers in the tetracene backbone (olive curve). This analysis shows that the resonances at lowest energy (284.5–285 eV) indeed result from excitations of carbon atoms in the tetracene backbone. Also the electron density in the corresponding final states is almost completely localized in the tetracene backbone while no appreciable density is found in the phenyl groups (cf. Figure 5c (i)). In the region of the second-lowest peak, however, not only contributions from excitations of tetracene core electrons but also from the innermost carbon atom of the phenyl side groups (carbon atom 6) are found. Moreover, even the strongest resonance at about 288.2 eV embraces individual resonances from both, the phenyl groups and the tetracene backbone (cf. Figure 5c (iii, iv) and Supporting Information), showing that the afore discussed very simple interpretation of the resonances based on isolated tetracene and PF-benzene spectra is not sufficient. Interestingly, the excitations of the carbon atoms in the phenyl groups at 286.3 and 288.2 eV end up in an equivalent final molecular orbital as visualized in Figure 5c (ii), (iii), hence demonstrating that the energetic difference between both resonances directly results from the aforementioned chemical shift between the carbon atoms 6 and 7–11. As shown exemplarily for the excited states presented in Figure 5c, the electron density is strictly limited to either the backbone or the phenyl groups depending on the respective excitation centers, demonstrating that the electronic systems of the molecular subunits are indeed decoupled from each other.

CONCLUSION

In summary, we have investigated partially fluorinated (F_{14}-RUB) and perfluorinated rubrene (PF-RUB) in thin films and solution with respect to their stability against oxidation. As we observe by real-time absorption experiments of thin films that were exposed to air for several hours, both the partially fluorinated F_{14}-RUB and the fully fluorinated PF-RUB are much more stable against oxygen than unsubstituted rubrene. Moreover, using NEXAFS spectroscopy combined with DFT computations we have analyzed the electronic structure and thin film orientation particularly of PF-RUB and we show that the molecules have not undergone a chemical reaction with oxygen. While oxidation of the thin films through oxygen has been investigated in the solid state, the electrochemical behavior (oxidation/reduction) in solution has been examined by cyclic voltammetric measurements. In addition, we further investigated the reduction and oxidation potentials of the three compounds in solution by comparison with DFT calculations. Both, experiments in the solid state and in solution show that the fully fluorinated PF-RUB is much more and the partially fluorinated F_{14}-RUB is considerably more stable than RUB, due to an increased oxidation potential. A systematic tunability of the oxidation potential depending on the degree of fluorination is in good agreement with observations from other rubrene derivatives with less fluorine.[16,17]

As a consequence, we believe that both fluorinated rubrene derivatives are promising candidates as an alternative to unsubstituted rubrene (RUB) in terms of stability against

DOI: 10.1021/acs.jpcc.5b12293
J. Phys. Chem. C 2016, 120, 5515–5522

photooxidation processes in organic electronics, since both F_{14}-RUB and PF-RUB have sterical and optical properties that are very similar to RUB. Hence, it would be vitally important to measure the transport properties of the fluoriated rubrenes in order to investigate whether these new compounds show similarly high charge carrier mobilities.[2,3] By now, it can be speculated that, due to their reduced susceptibility to oxygen, devices made of fluorinated rubrene would require less protection against ambient influence than common RUB devices.

■ ASSOCIATED CONTENT

Supporting Information

The Supporting Information is available free of charge on the ACS Publications website at DOI: 10.1021/acs.jpcc.5b12293.

Anodic cyclic voltammograms of RUB recorded with different scan rates (potential window of −0.34 to +1.26 V); cathodic cyclic voltammograms of F_{14}-RUB recorded with different scan rates (potential window of −0.35 to −2.45 V); computed NEXAFS spectra of PF-RUB for twisted and planar configuration; individual resonances of the spectrum computed for the planar geometry (PDF)

■ AUTHOR INFORMATION

Corresponding Author

*E-mail: Frank.Schreiber@uni-tuebingen.de.

Present Address

[⊥]Analytische Chemie, Ruhr-Universität-Bochum, Universitätsstr. 150, 44780 Bochum, Germany.

Notes

The authors declare no competing financial interest.

■ ACKNOWLEDGMENTS

We thank T. Suzuki for providing the material (F_{14}-RUB and PF-RUB). We gratefully thank the bwGRiD project[49] for the computational resources. We acknowledge the Helmholtz-Zentrum Berlin - Electron storage ring BESSY II for provision of synchrotron radiation at beamline HE-SGM. Furthermore, the DFG is acknowledged for funding within the Emmy Noether program.

■ REFERENCES

(1) Briseno, A. L.; Mannsfeld, S. C. B.; Ling, M. M.; Liu, S.; Tseng, R. J.; Reese, C.; Roberts, M. E.; Yang, Y.; Wudl, F.; Bao, Z. Patterning Organic Single-crystal Transistor Arrays. *Nature* **2006**, *444*, 913−917.

(2) Podzorov, V.; Menard, E.; Borissov, A.; Kiryukhin, V.; Rogers, J. A.; Gershenson, M. E. Intrinsic Charge Transport on the Surface of Organic Semiconductors. *Phys. Rev. Lett.* **2004**, *93*, 086602.

(3) Sundar, V. C.; Zaumseil, J.; Podzorov, V.; Menard, E.; Willett, R. L.; Someya, T.; Gershenson, M. E.; Rogers, J. A. Elastomeric Transistor Stamps: Reversible Probing of Charge Transport in Organic Crystals. *Science* **2004**, *303*, 1644−1646.

(4) Takeya, J.; Yamagishi, M.; Tominari, Y.; Hirahara, R.; Nakazawa, Y.; Nishikawa, T.; Kawase, T.; Shimoda, T.; Ogawa, S. Very High-Mobility Organic Single-Crystal Transistors with in-Crystal Conduction Channels. *Appl. Phys. Lett.* **2007**, *90*, 102120.

(5) Takeya, J.; Kato, J.; Hara, K.; Yamagishi, M.; Hirahara, R.; Yamada, K.; Nakazawa, Y.; Ikehata, S.; Tsukagoshi, K.; Aoyagi, Y.; et al. In-Crystal and Surface Charge Transport of Electric-Field-Induced Carriers in Organic Single-Crystal Semiconductors. *Phys. Rev. Lett.* **2007**, *98*, 196804.

(6) Podzorov, V.; Menard, E.; Pereversev, S.; Yakshinsky, B.; Madey, T.; Rogers, J. A.; Gershenson, M. E. Interaction of Organic Surfaces with Active Species in the High-vacuum Environment. *Appl. Phys. Lett.* **2005**, *87*, 093505.

(7) Bowen, E. J.; Steadman, F. 233. The Photo-oxidation of Rubrene. *J. Chem. Soc.* **1934**, 1098−1101.

(8) Nakayama, Y.; Machida, S.; Minari, T.; Tsukagishi, K.; Noguchi, Y.; Ishii, H. Direct Observation of the Electronic States of Single Crystalline Rubrene under Ambient Condition by Photoelectron Yield Spectroscopy. *Appl. Phys. Lett.* **2008**, *93*, 173305.

(9) Helou, M. E.; Medenbach, O.; Witte, G. Rubrene Microcrystals: A Route to Investigate Surface Morphology and Bulk Anisotropies of Organic Semiconductors. *Cryst. Growth Des.* **2010**, *10*, 3496−3501.

(10) Käfer, D.; Witte, G. Growth of Crystalline Rubrene Films with Enhanced Stability. *Phys. Chem. Chem. Phys.* **2005**, *7*, 2850−2853.

(11) Kowarik, S.; Gerlach, A.; Sellner, S.; Schreiber, F.; Pflaum, J.; Cavalcanti, L.; Konovalov, O. Anomalous Roughness Evolution of Rubrene Thin Films Observed in Real Time during Growth. *Phys. Chem. Chem. Phys.* **2006**, *8*, 1834−1836.

(12) McGarry, K. A.; Xie, W.; Sutton, C.; Risko, C.; Wu, Y.; Young, V. G.; Brédas, J.-L.; Frisbie, C. D.; Douglas, C. J. Rubrene-Based Single-Crystal Organic Semiconductors: Synthesis, Electronic Structure, and Charge-Transport Properties. *Chem. Mater.* **2013**, *25*, 2254−2263.

(13) Mamada, M.; Katagiri, H.; Sakanoue, T.; Tokito, S. Characterization of New Rubrene Analogues with Heteroaryl Substituents. *Cryst. Growth Des.* **2015**, *15*, 442−448.

(14) Uttiya, S.; Miozzo, L.; Fumagalli, E. M.; Bergantin, S.; Ruffo, R.; Parravicini, M.; Papagni, A.; Moret, M.; Sassella, A. Connecting Molecule Oxidation to Single Crystal Structural and Charge Transport Properties in Rubrene Derivatives. *J. Mater. Chem. C* **2014**, *2*, 4147−4155.

(15) Zhang, X.; Sørensen, J. K.; Fu, X.; Zhen, Y.; Zhao, G.; Jiang, L.; Dong, H.; Liu, J.; Shuai, Z.; Geng, H.; et al. Rubrene Analogues with the Aggregation-induced Emission Enhancement Behaviour. *J. Mater. Chem. C* **2014**, *2*, 884−890.

(16) Paraskar, A. S.; Reddy, A. R.; Patra, A.; Wijsboom, Y. H.; Gidron, O.; Shimon, L. J. W.; Leitus, G.; Bendikov, M. Rubrenes Planar and Twisted. *Chem. - Eur. J.* **2008**, *14*, 10639−10647.

(17) Uttiya, S.; Raimondo, L.; Campione, M.; Miozzo, L.; Yassar, A.; Moret, M.; Fumagalli, E.; Borghesi, A.; Sassella, A. Stability to Photo-Oxidation of Rubrene and Fluorine-Substituted Rubrene. *Synth. Met.* **2012**, *161*, 2603−2606.

(18) Mullenbach, T. K.; McGarry, K. A.; Luhman, W. A.; Douglas, C. J.; Holmes, R. J. Connecting Molecular Structure and Exciton Diffusion Length in Rubrene Derivatives. *Adv. Mater.* **2013**, *25*, 3689−3693.

(19) Hinderhofer, A.; Heinemeyer, U.; Gerlach, A.; Kowarik, S.; Jacobs, R. M. J.; Sakamoto, Y.; Suzuki, T.; Schreiber, F. Optical Properties of Pentacene and Perfluoropentacene Thin Films. *J. Chem. Phys.* **2007**, *127*, 194705.

(20) Kowarik, S.; Gerlach, A.; Hinderhofer, A.; Milita, S.; Borgatti, F.; Zontone, F.; Suzuki, T.; Biscarini, F.; Schreiber, F. Structure, Morphology, and Growth Dynamics of Perfluoro-pentacene Thin Films. *Phys. Status Solidi RRL* **2008**, *2*, 120−122.

(21) Duhm, S.; Hosoumi, S.; Salzmann, I.; Gerlach, A.; Oehzelt, M.; Wedl, B.; Lee, T.-L.; Schreiber, F.; Koch, N.; Ueno, N.; et al. Influence of Intramolecular Polar Bonds on Interface Energetics in Perfluoropentacene on Ag(111). *Phys. Rev. B: Condens. Matter Mater. Phys.* **2010**, *81*, 045418.

(22) Koch, N.; Gerlach, A.; Duhm, S.; Glowatzki, H.; Heimel, G.; Vollmer, A.; Sakamoto, Y.; Suzuki, T.; Zegenhagen, J.; Rabe, J. P.; et al. Adsorption Induced Intramolecular Dipole: Correlating Molecular Conformation and Interface Electronic Structure. *J. Am. Chem. Soc.* **2008**, *130*, 7300−7304.

(23) Anger, F.; Ossó, J. O.; Heinemeyer, U.; Broch, K.; Scholz, R.; Gerlach, A.; Schreiber, F. Photoluminescence Spectroscopy of Pure Pentacene, Perfluoropentacene, and Mixed Thin Films. *J. Chem. Phys.* **2012**, *136*, 054701.

(24) Anger, F.; Scholz, R.; Adamski, E.; Broch, K.; Gerlach, A.; Sakamoto, Y.; Suzuki, T.; Schreiber, F. Optical Properties of Fully and Partially Fluorinated Rubrene in Films and Solution. *Appl. Phys. Lett.* **2013**, *102*, 013308.

(25) Suzuki, T.; Sakamoto, Y. *Development of Organic Semiconductors for Molecular Thin-Film Devices*; Institute for Molecular Science: Myodaiji, Japan, 2013; pp 84−85.
(26) Gritzner, G.; Kůta, J. Recommendations on Reporting Electrode Potentials in Nonaqueous Solvents (Recommendations 1983). *Pure Appl. Chem.* **1984**, *56*, 461−466.
(27) TURBOMOLE V6.4 2012, a development of University of Karlsruhe and Forschungszentrum Karlsruhe GmbH, 1989−2007, TURBOMOLE GmbH, since 2007; available from http://www.turbomole.com.
(28) Kytka, M.; Gerlach, A.; Kováč, J.; Schreiber, F. Real-time Observation of Oxidation and Photo-oxidation of Rubrene Thin Films by Spectroscopic Ellipsometry. *Appl. Phys. Lett.* **2007**, *90*, 131911.
(29) Hermann, K., Pettersson, L. G. M., Casida, M. E., Daul, C., Goursot, A., Koester, A., Proynov, E., St-Amant, A., Salahub, D. R. Contributing authors: Carravetta, V., Duarte, H., Friedrich, C., Godbout, N., Guan, J., Jamorski, C., Leboeuf, M., Leetmaa, M., Nyberg, M., Patchkovskii, S., Pedocchi, L., Sim, F., Triguero, L., Vela, A. StoBe-deMon version 3.2, 2013.
(30) Klues, M.; Hermann, K.; Witte, G. Analysis of the Near-edge X-ray-absorption Fine-structure of Anthracene: A Combined Theoretical and Experimental Study. *J. Chem. Phys.* **2014**, *140*, 014302.
(31) Heinze, J. Cyclic Voltammetry-"Electrochemical Spectroscopy". *Angew. Chem., Int. Ed. Engl.* **1984**, *23*, 831−847.
(32) Cardona, C. M.; Li, W.; Kaifer, A. E.; Stockdale, D.; Bazan, G. C. Electrochemical Considerations for Determining Absolute Frontier Orbital Energy Levels of Conjugated Polymers for Solar Cell Applications. *Adv. Mater.* **2011**, *23*, 2367−2371.
(33) Kapturkiewicz, A. Solvent and Temperature Control of the Reaction Mechanism and Efficiency in the Electrogenerated Chemiluminescence of Rubrene. *J. Electroanal. Chem.* **1994**, *372*, 101−116.
(34) Yamaguchi, Y. Effects of Fluorination on Electronic and Excited States of Fused Zinc Oligoporphyrins. *J. Chem. Phys.* **2005**, *122*, 184702.
(35) Anger, F.; Glowatzki, H.; Franco-Cañellas, A.; Bürker, C.; Gerlach, A.; Scholz, R.; Sakamoto, Y.; Suzuki, T.; Koch, N.; Schreiber, F. Interface Dipole and Growth Mode of Partially and Fully Fluorinated Rubrene on Au(111) and Ag(111). *J. Phys. Chem. C* **2015**, *119*, 6769−6776.
(36) Sakamoto, Y.; Suzuki, T.; Kobayashi, M.; Gao, Y.; Inoue, Y.; Tokito, S. Perfluoropentacene and Perfluorotetracene: Syntheses, Crystal Structures, and FET Characteristics. *Mol. Cryst. Liq. Cryst.* **2006**, *444*, 225−232.
(37) Harada, Y.; Takahashi, T.; Fujisawa, S.; Kajiwara, T. Application of Photoelectron Spectroscopy to the Study of Photochemical Reactions of Solids. Photooxidation of Rubrene (5,6,11,12-tetraphenylnaphthacene). *Chem. Phys. Lett.* **1979**, *62*, 283−286.
(38) Anger, F.; Scholz, R.; Gerlach, A.; Schreiber, F. Vibrational Modes and Changing Molecular Conformation of Perfluororubrene in Thin Films and Solution. *J. Chem. Phys.* **2015**, *142*, 224703.
(39) Hill, I. G.; Kahn, A.; Soos, Z. G.; Pascal, R. A., Jr. Charge-separation Energy in Films of π-conjugated Organic Molecules. *Chem. Phys. Lett.* **2000**, *327*, 181−188.
(40) Scholz, R.; Luschtinetz, R.; Seifert, G.; Jägeler-Hoheisel, T.; Körner, C.; Leo, K.; Rapacioli, M. Quantifying Charge Transfer Energies at Donor-acceptor Interfaces in Small-molecule Solar Cells with Constrained DFTB and Spectroscopic Methods. *J. Phys.: Condens. Matter* **2013**, *25*, 473201.
(41) Hofmann, S.; Hummert, M.; Scholz, R.; Luschtinetz, R.; Murawski, C.; Will, P.-A.; Hintschich, S. I.; Alex, J.; Jankus, V.; Monkman, A. P.; et al. Engineering Blue Fluorescent Bulk Emitters for OLEDs: Triplet Harvesting by Green Phosphors. *Chem. Mater.* **2014**, *26*, 2414−2426.
(42) Käfer, D.; Ruppel, L.; Witte, G.; Wöll, C. Role of Molecular Conformations in Rubrene Thin Film Growth. *Phys. Rev. Lett.* **2005**, *95*, 166602.
(43) Vijayalakshmi, S.; Föhlisch, A.; Kirchmann, P.; Hennies, F.; Pietzsch, A.; Nagasono, M.; Wurth, W. Bond Polarization and Image-potential Screening in Adsorbed C_6F_6 on Cu(111). *Surf. Sci.* **2006**, *600*, 4972−4977.
(44) Breuer, T.; Klues, M.; Witte, G. Characterization of Orientational Order in π-conjugated Molecular Thin Films by NEXAFS. *J. Electron Spectrosc. Relat. Phenom.* **2015**, *204*, 102−115.
(45) Stöhr, J., Ed.; *NEXAFS Spectroscopy*; Springer-Verlag: Berlin, 1992.
(46) Wang, L.; Chen, S.; Liu, L.; Qi, D.; Gao, X.; Subbiah, J.; Swaminathan, S.; Wee, A. T. S. Conformational Degree and Molecular Orientation in Rubrene Film by in Situ X-ray Absorption Spectroscopy. *J. Appl. Phys.* **2007**, *102*, 063504.
(47) Song, X.; Wang, L.; Fan, Q.; Wu, Y.; Wang, H.; Liu, C.; Liu, N.; Zhu, J.; Qi, D.; Gao, X.; et al. Role of Oxygen Incorporation in Electronic Properties of Rubrene Films. *Appl. Phys. Lett.* **2010**, *97*, 032106.
(48) Sinha, S.; Wang, C.-H.; Mukherjee, M.; Mukherjee, T.; Yang, Y.-W. Oxidation of Rubrene Thin Films: An Electronic Structure Study. *Langmuir* **2014**, *30*, 15433−15441.
(49) bwGRiD (http://www.bw-grid.de), member of the German D-Grid initiative, funded by the Ministry for Education and Research (Bundesministerium für Bildung und Forschung) and the Ministry for Science, Research and Arts Baden-Württemberg (Ministerium für Wissenschaft, Forschung und Kunst Baden-Württemberg).

DOI: 10.1021/acs.jpcc.5b12293
J. Phys. Chem. C 2016, 120, 5515−5522